



1 **Real-time prediction of rain-triggered lahars: incorporating 2 seasonality and catchment recovery**

3 Robbie Jones^{a*}, Vern Manville^a, Jeff Peakall^a, Melanie Froude^{bc}, Henry Odber^{de}

4 ^aSchool of Earth and Environment, University of Leeds, Leeds. LS2 9JT, United Kingdom

5 ^bSchool of Environmental Sciences, University of East Anglia, Norwich, NR4 7TJ, United Kingdom

6 ^cDepartment of Geography, University of Sheffield, 9 Northumberland Road, Sheffield, S10, UK

7 ^dSchool of Earth Sciences, University of Bristol, Wills Memorial Building, Queens Road, Bristol BS8 1RJ, United
8 Kingdom

9 ^eMet Office, FitzRoy Road, Exeter, Devon, EX1 3PB, United Kingdom

10 *Correspondence to: Robbie Jones (eerj@leeds.ac.uk)

11 **Abstract.** Rain-triggered lahars are a significant secondary hydrological and geomorphic hazard at volcanoes
12 where unconsolidated pyroclastic material produced by explosive eruptions is exposed to intense rainfall, often
13 occurring for years to decades after the initial eruptive activity. Previous studies have shown that secondary lahar
14 initiation is a function of rainfall parameters, source material characteristics and time since eruptive activity. In
15 this study, probabilistic rain-triggered lahar forecasting models are developed using the lahar occurrence and
16 rainfall record of the Belham River Valley at Soufrière Hills Volcano, Montserrat collected between April 2010
17 and April 2012. In addition to the use of peak rainfall intensity as a base forecasting parameter, considerations for
18 the effects of rainfall seasonality and catchment evolution upon the initiation of rain-triggered lahars and the
19 predictability of lahar generation are also incorporated into these models. Lahar probability increases with peak
20 one-hour rainfall intensity throughout the two-year dataset, and is higher under given rainfall conditions in year
21 one than year two. The probability of lahars is also enhanced during the wet season, when large-scale synoptic
22 weather systems (including tropical cyclones) are more common and antecedent rainfall and thus levels of deposit
23 saturation are typically increased. The incorporation of antecedent conditions and catchment evolution into
24 logistic regression-based rain-triggered lahar probability estimation models is shown to enhance model
25 performance and displays the potential for successful real-time prediction of lahars, even in areas featuring
26 strongly seasonal climates and temporal catchment recovery.

27 **1 Introduction**

28 Lahars are rapidly flowing mixtures of rock debris and water (other than normal streamflow) from a volcano and
29 represent a significant hazard due to their energetic nature and mobility (Smith and Fritz, 1989). Globally, 17%
30 of historical volcano-related fatalities have occurred due to lahars (Auker et al., 2013); with decadal-scale hazards
31 being created by some large eruptions (Major et al., 2000). Secondary, post-eruption lahars are dominantly the
32 result of rainfall on unconsolidated pyroclastic deposits, which are typically remobilised by rilling due to
33 Hortonian overland flow (Segerstrom, 1950; Waldron, 1967) or by shallow landsliding of saturated tephra layers
34 above basal décollement surfaces (Iverson, 2000; Manville et al., 2000).

35 At present, rain-triggered lahar hazard identification is predominantly based on observations as well as ground-
36 based flow detection systems such as Acoustic Flow Monitors (AFMs) or trip-wires at locations where such
37 resources are available (e.g. Marcial et al., 1996; Lavigne et al., 2000). Previous studies featuring post-lahar



38 analysis of flow observations and rainfall records at a range of volcanoes have displayed a power-law relationship
39 indicating that lahar initiation occurs along a continuum from short duration, high intensity rainfall events to long
40 duration, low-intensity events (e.g. Rodolfo and Arguden, 1991; Capra et al., 2010; Jones et al., 2015). Enhancing
41 the use of local telemetered rainfall gauge networks within lahar hazard monitoring and assessment has the
42 potential to increase the number of available mitigation tools whilst avoiding the lag-time between flow initiation
43 and flow detection inherent in ground-based detection and observation. Globally, such pre-emptive prediction and
44 forecasting of rain-triggered lahars based on telemetered rainfall data is lacking, although initial application of
45 real-time rainfall data for lahar prediction has demonstrated increased lahar warning times compared with ground-
46 based flow detection (Jones et al., 2015).
47 The initiation of rain-triggered lahars is dependent on the characteristics of rainfall, pyroclastic deposits and
48 topography, indicating that both the climatic regime of lahar-prone regions and the hydrogeomorphic response of
49 drainage basins to eruptive activity are important considerations in rain-triggered lahar research (Pierson and
50 Major, 2014). Regions of high rainfall seasonality are predominantly distributed in the tropics and sub-tropics
51 either side of the equator (Wang et al., 2010); whilst approximately 46% of active volcanoes are identified as
52 being located in the humid tropics (Rodolfo and Arguden, 1991). Despite this geographic coincidence and the
53 importance of climatic rainfall regimes on storm intensities, durations and antecedent conditions, all significant
54 factors in lahar initiation (Pierson and Major, 2014), the impact of seasonal rainfall on rain-triggered lahar
55 initiation has not previously been explicitly considered within the development of rain-triggered lahar hazard
56 assessment tools.
57 Following a discrete volcanic eruption, sediment yields in impacted fluvial systems are amongst the highest
58 recorded globally, but decline exponentially (Major et al., 2000), which is consistent with other examples of
59 disturbed earth systems (Graf, 1977). Mechanisms include a reduction in available particulate material, vegetation
60 recovery, fragmentation of runoff-enhancing surface crusts, exposure of more permeable substrates and the
61 stabilisation of rill networks (Leavesley et al., 1989; Schumm and Rea, 1995; Major et al., 2000; Major and
62 Yamakoshi, 2005). Conversely, at locations featuring recurrent or persistent volcanic activity, the magnitude of
63 the lahar hazard remains relatively constant with time due to the regular supply of new material (Thouret et al.,
64 2014). As a result, temporal catchment development is another factor which influences lahar frequency and
65 magnitude, indicating that it is also an important consideration within the development of rain-triggered lahar
66 hazard assessment tools.
67 This study uses probabilistic and diagnostic methods, including binary logistic regression and Receiver Operating
68 Characteristic (ROC) analysis, to develop real-time rainfall-based lahar forecasting tools which account for the
69 impacts of seasonal rainfall and catchment recovery on lahar occurrence in the Belham Valley, Montserrat. Such
70 hazard assessment tools have the potential to be utilised both as a stand-alone tool where ground-based detection
71 equipment is unavailable, and in conjunction with instrumental monitoring techniques to increase lahar warning
72 times.

73 **2 Soufrière Hills Volcano, Montserrat**

74 Soufrière Hills Volcano (SHV, Montserrat, Lesser Antilles, 16.72°N, 62.18°W) lies on the northern edge of the
75 Inter-Tropical Convergence Zone in the eastern Caribbean and has a strongly seasonal climate. Rainfall-producing
76 weather systems affecting the island fall into two broad categories; large-scale synoptic (>100 km across) systems



77 and local mesoscale (<100 km across) systems (Froude, 2015). Both can produce high intensity precipitation, but
78 large-scale events can potentially be forecast days in advance whereas this timescale reduces to hours for local
79 weather systems (Barclay et al., 2006).
80 The andesitic dome-forming eruption of SHV began in July 1995 and has featured several phases of activity
81 consisting of dome growth, dome collapse and vulcanian explosions as well as pauses in magma extrusion
82 (Bonadonna et al., 2002; Komorowski et al., 2010; Stinton et al., 2014). Pyroclastic density currents (PDCs) have
83 deposited fine-grained ash- and pumice-rich and coarser-grained blocky deposits around the volcano (Cole et al.,
84 2002; Stinton et al., 2014), supplemented by tephra deposits from short-lived Vulcanian explosions and associated
85 fountain-collapse flows and surges (Komorowski et al., 2010). Prevailing winds often distribute ash from weak
86 plumes to the West, but larger plumes can also deposit to the North, East and South (Bonadonna et al., 2002).
87 This intermittent eruptive activity has triggered a complex sedimentological response in drainages surrounding
88 the volcano since 1995 (Barclay et al., 2006, 2007; Alexander et al., 2010; Froude, 2015).

89 **3 The Belham Catchment**

90 Data from the Belham Valley, Montserrat (Fig. 1) were used to examine the influence of rainfall seasonality and
91 catchment evolution on the occurrence of rain-triggered lahars between April 2010 and April 2012 (Fig. 2). Lahars
92 have persisted in the valley since the onset of eruptive activity in 1995 and have damaged infrastructure, including
93 burying the Belham Bridge in 1998, resulting in the river bed being used as the primary transportation link between
94 the “Safe Zone” and the “Daytime Entry Zone” (Barclay et al., 2007; Alexander et al., 2010).

95 The Belham Catchment had a pre-1995 surface area of c. 13.7 km², increasing to c. 14.8 km² early in the eruptive
96 episode due to capture of a portion of Gage’s fan (Froude, 2015). During eruptive episodes tephra fall and
97 pyroclastic density current (PDC) deposits accumulate in the upper catchment. The destruction and burial of
98 vegetation in the Belham Valley reduces the infiltration and interception of precipitation, and in combination with
99 a reduction in surface roughness enhances run-off and erosion rates and promotes rain-triggered lahar generation
100 (Barclay et al., 2007; Alexander et al., 2010; Froude, 2015). Aggradation and sedimentation in the upper
101 catchment during periods of eruptive activity are counter-balanced during periods of quiescence by channel
102 development and stabilisation, exposure of more permeable substrates, vegetation recovery and a reduction in
103 available sediment (Froude, 2015). The data period used here coincides with a lack of substantial eruptive activity
104 at SHV following the 11th of February 2010 dome collapse at the end of “Phase 5”, which deposited stacked lobes
105 of pumiceous PDC deposits up to 5.7 km from source in the Belham Valley (Stinton et al., 2014). This period of
106 eruptive quiescence indicates that this study focuses on a time of channel development and stabilisation within
107 the upper catchment of the Belham Valley.

108 **4 Rainfall and Lahar Record**

109 The record used in this study (Fig. 2) comprises 0.1 mm resolution hourly precipitation data recorded at the MVO
110 Helipad Gauge between February 2010 and February 2011, the St George’s Hill gauge between March 2011 and
111 May 2011, and the maximum of the St George’s Hill and Windy Hill gauges (Fig. 1) between May 2011 and
112 February 2012. The lahar database (Fig. 2) is compiled from inspection of seismic records and visual observations.
113 Lahar size (small, medium, large) is estimated based on recorded seismic amplitude and occupied valley width



114 alongside flow start time, end time and duration. Division of the dataset into six-month moving windows, with
115 staggered one-month start dates, facilitates the illustration of the seasonal variation in both the number of rainfall
116 events exceeding One Hour Peak Rainfall Intensity (1hrPRI: the highest resolution available) thresholds and the
117 occurrence (and estimated magnitude) of lahars (Fig. 3).

118 **5 Results**

119 The six-month window between April and October is identified as the peak wet season in this study, with 1721
120 mm of recorded rainfall in the 2010 peak wet season (WS1) and 1455 mm in the 2011 peak wet season (WS2).
121 The 2010/11 peak dry season (DS1) featured approximately 750 mm of rainfall, whilst 1076 mm of rainfall was
122 recorded in the 2011/12 peak dry season (DS2). Mean WS1 and WS2 1hrPRIs are 5.2 mm hr^{-1} and 5.0 mm hr^{-1}
123 respectively, whilst mean dry season 1hrPRIs are 2.2 mm hr^{-1} (DS1) and 3.3 mm hr^{-1} (DS2).
124 There is significant ($p < 0.01$) correlation between recorded rainfall on timescales of 1-168 hours and lahar
125 occurrence. When lahars are categorised by estimated magnitude, large lahars are strongly correlated with longer-
126 duration (>24 hours) rainfall events, produced by the passage of synoptic weather systems. Between April 2010
127 and April 2012 large flows were directly attributed to several named tropical cyclones (Fig. 2). In contrast, smaller
128 lahars display increased correlation with the passage of short-duration (<24 hours) rainfall events, more commonly
129 associated with mesoscale weather systems.

130 **5.1 Probabilistic rain-triggered lahar analysis**

131 The correlation between peak rainfall intensity and lahar occurrence provides the platform for
132 probabilistic analysis of lahar occurrence based on the 1hrPRI of a rainfall event. Within this study a designated
133 minimum inter-event dry period of six hours is utilised, meaning that in common with several previous soil erosion
134 studies a dry interval of six hours is needed to define the end of a single rainfall event (Wischmeier and Smith
135 1978; Todisco, 2014). Results show that lahar probability increases with greater 1hrPRI in both years of the
136 Belham Valley dataset, with higher lahar probabilities in year 1 than year 2 for a given 1hrPRI (Fig. 4).

137 Empirically-derived lahar probabilities for rainfall events featuring a given minimum 1hrPRI fluctuate seasonally
138 during the study period (Fig. 5). These 1hrPRI exceedance-based lahar probabilities (Fig. 5) are initially stable
139 during the 6-month windows focused on WS1 before decreasing during DS1, increasing during WS2 and once
140 again decreasing into DS2. This indicates that more intense rainfall is required to trigger lahars in the dry season
141 than in the wet season. Throughout the two-year study period increased 1hrPRI correlates with increased lahar
142 probability, displaying its effectiveness as a potential first-order lahar forecasting parameter.

143 In addition to seasonal fluctuations in relative lahar probability, there is an overall decline in relative lahar
144 probabilities across the two-year study period (Figs. 4 & 5). The combination of seasonal fluctuation and temporal
145 decline in lahar probability displayed in Figure 5 is examined further using binary logistic regression, a statistical
146 method which estimates the probability of a dichotomous outcome using one or more independent variables
147 (Hosmer Jr et al., 2013). In this instance the occurrence or non-occurrence of lahars (of any magnitude) is used as
148 the dichotomous dependent variable and initially the 1hrPRI of a rainfall event is the singular independent
149 variable. Figure 6A displays logistic regression-based lahar probability estimation models generated by this
150 approach using four sub-datasets; *Year 1*, *Year 2*, *Wet Seasons* and *Dry Seasons*. Within each of these four models



151 the model chi-square test indicated statistically significant lahar prediction ability ($p < 0.01$). Figure 6A displays
152 higher estimated lahar probabilities at identical 1hrPRI values for Year 1 relative to Year 2 and Wet Seasons
153 relative to Dry Seasons.
154 The potential benefit of incorporating considerations for seasonal and temporal effects within lahar forecasting
155 models was investigated using further binary logistic regression. This approach selected alternate chronological
156 rainfall events (minimum total rainfall ≥ 8 mm) from the two-year dataset, creating a model formulation dataset
157 consisting of 74 rainfall events, of which 25 produced lahars. Lahar forecasting models were created from this
158 model formulation dataset using binary logistic regression, and the remaining 73 rainfall events, of which 20
159 produced lahars, were retained for the assessment of the performance of the lahar forecasting models. Proxies for
160 seasonal effects (antecedent rainfall on timescales of 1-90 days) and catchment recovery (long-term cumulative
161 rainfall and days since significant eruptive activity) were tested in combination with 1hrPRI. The minimum event
162 rainfall threshold of 8 mm (under which only two lahars occurred during the two-year dataset) was implemented
163 for logistic regression and subsequent forecasting assessment in order to increase the balance between lahar and
164 non-lahar outcomes and thus reduce skewed predicted probability.
165 Three-day antecedent rainfall displayed the biggest influence of the tested antecedent rainfall timescales upon the
166 effectiveness of lahar forecasts, while total cumulative rainfall since significant eruptive activity best captured
167 temporal catchment development effects. Therefore, the optimal lahar forecasting model developed from the
168 model formulation dataset utilises 3-day antecedent rainfall and long-term cumulative rainfall alongside the first-
169 order lahar forecasting parameter of 1hrPRI. The reverse stepwise logistic regression method (Hosmer Jr et al.,
170 2013), which involves the deletion of variables whose removal from the model results in a statistically
171 insignificant deterioration of model performance, retained these three independent variables. This model
172 composition increased correct classification of rainfall event outcomes in the model formulation dataset from a
173 null model value of 66% (when all events in the database are predicted to not trigger lahars) to 80% when using
174 our explanatory variables, with model chi-square tests again indicating significant prediction ability ($p < 0.01$).
175 Model variables (X_i) and output regression coefficients (β_i) are used to construct lahar probability estimation
176 equations by conversion of the logistic regression logit model (Eq. 1) in terms of probability.
177 (1)
$$\text{logit}(p) = \beta_0 + \beta_1 X_1 + \beta_2 X_2 + \dots + \beta_n X_n$$

178 Eq. 2 displays the application of this to the multi-variable model, featuring the probability of lahar occurrence (p),
179 1hrPRI (R_i), three-day antecedent rainfall (A_3) and cumulative rainfall since significant eruptive activity (C).
180 (2)
$$p = \frac{1}{1 + e^{(-2.10 + 0.133R_i + 0.018A_3 - 0.215C)}}$$

181 Eq. 3 displays the lahar probability estimation model produced by the same dataset using only 1hrPRI as an
182 independent variable.
183 (3)
$$p = \frac{1}{1 + e^{(-2.33 + 0.133R_i)}}$$

184 Application of Eqs. 2 & 3 to the 73 rainfall events in the forecasting assessment dataset produced two sets of
185 model-derived lahar probability estimates. The lahar forecasting performance of the two models was then assessed
186 relative to the actual outcomes (lahar or no lahar) of the rainfall events using Receiver Operating Characteristic
187 (ROC) analysis (Fawcett, 2006). ROC analysis plots the true positive rate against the false positive rate as a
188 threshold (estimated lahar probability) is varied in order to assess its ability to discriminate between lahar and
189 non-lahar producing rainfall events. The area under the ROC curve (AUC) is a measure of the ability of a tool to



190 distinguish between the two outcomes, and varies between 0.5 (no predictive ability) and 1.0 (perfect predictive
191 ability). The multiple-variable lahar probability estimation model shown in Eq. 2 produced an AUC of 0.83
192 ($p < 0.01$), whilst the single variable model shown in Eq. 3 produced an AUC of 0.79 ($p < 0.01$) (Fig. 6B). The AUC
193 produced by Eq. 2 increases to 0.93 if the 8 mm event threshold is removed and the multi-variable model is applied
194 to all 508 rainfall events that were not used in model formulation.

195 **6 Discussion**

196 Analysis of the Belham Valley lahar occurrence and rainfall record over a two-year period indicates that lahar
197 probability and magnitude is a function of: (i) temporal catchment evolution towards more stable conditions –
198 lahar are harder to trigger with time; and (ii) seasonal variations in rainfall – lahar are more common in the wet
199 season both in terms of frequency and probability relative to 1hrPRI.

200 The multi-year temporal trend is attributed to a declining supply of easily erodible pyroclastic material in the
201 upper catchment, coupled with stabilisation of channel networks, vegetation re-growth, and increased infiltration
202 as identified in several previous studies of lahar-prone regions following eruptive activity (e.g. Leavesley et al.,
203 1989; Schumm and Rea, 1995; Major et al., 2000; Major and Yamakoshi, 2005). The occurrence of several large
204 rainfall events following Phase 5 of the eruption (Fig. 2) triggered a number of high-magnitude lahar within the
205 Belham Valley, enhancing temporal channel development within the catchment and resulting in the widespread
206 erosion and downstream transportation of pyroclastic material (Froude, 2015). Rapid re-vegetation during periods
207 of eruptive quiescence has also been identified in the catchment (Froude, 2015), a process which increases
208 infiltration, interception, evapotranspiration and surface roughness; reducing post-eruption runoff rates
209 (Yamakoshi and Suwa, 2000; Ogawa et al., 2007; Alexander et al., 2010). Temporal increase in infiltration rates
210 in the Belham Valley is also attributed to the exposure of more permeable substrates following the erosion of fine-
211 grained surface tephra layers (Froude, 2015), a factor identified previously in studies of the landscape response to
212 the 1980 eruption of Mt St Helens (Collins and Dunne, 1986; Leavesley et al., 1989).

213 Probabilistic analysis shows that throughout the two-year dataset utilised in this study, increased 1hrPRI results
214 in increased lahar occurrence probability. Additionally, an increase in the absolute numbers of lahar and a
215 reduction in rain-triggered lahar initiation thresholds are identified in the wet seasons. Seasonality in the nature
216 and frequency of rainfall-generating weather systems controls this pattern. Large lahar are often associated with
217 the passage of synoptic weather systems, which typically produce long-duration catchment-wide rainfall. This is
218 demonstrated by the triggering of large lahar by several named storms during the study dataset including
219 Hurricane Earl in August 2010, Tropical Storm Otto in October 2010 and Tropical Storm Maria in September
220 2011. Increased rainfall in the wet season also influences the dominant antecedent conditions within the
221 catchment, resulting in reduced infiltration rates due to deposit saturation (Barclay et al., 2007). Increased
222 antecedent rainfall can also produce runoff-enhancing surface seals (Segerstrom, 1950; Fohrer et al., 1999) and
223 result in increased bulking efficiency during lahar transit due to high water contents in channel floor deposits
224 (Iverson et al., 2011). These effects increase the overall probability of lahar in the wet season under given rainfall
225 conditions due to flash-flood type responses to rainfall. The absence of large lahar in the dry season is attributed
226 to the occurrence of fewer sustained catchment-wide synoptic weather systems as well as antecedent effects (low
227 antecedent rainfall inhibits bulking efficiency in the dry season). The development of lahar magnitude assessment
228 methods, from the subjective classification used in this study, towards quantitative initial flow volume estimates



229 has the potential to enhance probabilistic lahar forecasting by creating probabilistic hazard footprints (Mead et al.,
230 2016). However, such quantitative assessment methods are highly data intensive relative to those developed within
231 this study, requiring pre- and post-eruption digital elevation models, location specific rainfall intensity-frequency-
232 duration thresholds and physical deposit characteristics as input data (Mead et al., 2016). These input data
233 requirements prohibit practical implementation of fully-quantitative magnitude estimates within probabilistic
234 rain-triggered lahar assessment at all but the most thoroughly monitored volcanoes.
235 The incorporation of considerations for temporal catchment development and seasonality of prevalent antecedent
236 conditions into logistic regression-based lahar probability estimation models increases rain-triggered lahar
237 forecasting performance. The addition of these considerations modulates purely 1hrPRI-based probability
238 estimates to account for initial deposit moisture content and the degree of catchment recovery during a period of
239 eruptive quiescence. ROC analysis indicates an excellent ability to differentiate between lahar and non-lahar
240 outcomes (AUC = 0.83) when only larger rainfall events resulting in ≥ 8 mm of total rainfall are considered, and
241 this ability improves even further (AUC = 0.93) when the 8 mm threshold is removed. The readily available model
242 inputs of 1hrPRI, three-day antecedent rainfall and cumulative rainfall since significant eruptive activity can be
243 easily assimilated into functional real-time lahar probability estimation models and produces real benefits. Lahar
244 forecasting using real-time telemetered rainfall data and these techniques has the potential to effectively predict
245 secondary lahars and increase lahar warning times, even in areas where AFMs, proximal seismometers and trip
246 wires are unavailable. Used in conjunction with ground-based detectors in instrumented catchments lahar warning
247 times can be doubled (Jones et al., 2015).
248 Further research to expand the length of the current two-year study period would develop the understanding of
249 the catchment recovery-driven temporal trends in lahar occurrence identified within this study. Likewise, the
250 application of these techniques to additional volcanoes would facilitate both the further examination of the
251 performance of the lahar forecasting models and the investigation of other important parameters contributing to
252 the frequency and magnitude of rain-triggered lahar initiation.

253 **7 Conclusions**

254 This study demonstrates the development and enhancement of logistic regression-based rain-triggered lahar
255 probability estimation models for real-time lahar forecasting using the lahar occurrence and rainfall record of the
256 Belham Valley, Montserrat between April 2010 and April 2012. The incorporation of both antecedent rainfall and
257 considerations for temporal catchment development into such models alongside the first-order lahar forecasting
258 parameter of peak rainfall intensity is shown to improve lahar forecasting performance. Rainfall seasonality and
259 catchment recovery are identified as important factors in the severity of the rain-triggered lahar hazard at Soufrière
260 Hills Volcano, Montserrat, and by extension similar volcanoes worldwide. Seasonal influences increase both the
261 absolute number of lahars and the probability of lahar occurrence under pre-defined rainfall conditions during the
262 wet season due to antecedent effects. Lahar probability is also shown to decline with time under given antecedent
263 and peak rainfall intensity conditions as a product of catchment evolution. Our results demonstrate the potential
264 for successful real-time prediction of secondary lahars using readily available input data, even in areas featuring
265 strongly seasonal climates and periods of eruptive quiescence.



266 **Competing Interests**

267 The authors declare that they have no conflict of interest.

268 **Acknowledgements**

269 This research was supported by STREVA (NERC/ESRC consortium NE/J02483X/1) and we are thankful
270 to theMontserrat Volcano Observatory (MVO) for permission to use the lahar database and rain gauge dataset.



271 **Figure Captions**

272 **Figure 1: Location map of Montserrat and Soufrière Hills Volcano.**

273 **Figure 2: Timeline illustrating hourly rainfall data (above) and rain-triggered lahar activity (below) in the Belham**
274 **Valley, Montserrat between April 2010 and April 2012 (with minor gaps (shaded) due to equipment failure). S, M, and**
275 **L on the vertical axis represent Small, Medium and Large lahars respectively, see text for details.**

276 **Figure 3: Illustration of the seasonal fluctuations in lahar occurrence displayed using 6-month data windows with 1-**
277 **month staggered start dates. Vertical bars indicate the number of lahar events, categorised by magnitude, in each 6-**
278 **month period. Background contours display the number of rainfall events exceeding specified Peak One Hour Rainfall**
279 **Intensity (1hrPRI) thresholds, in each 6-month period.**

280 **Figure 4: Lahar probability, classified by magnitude, as categorised One Hour Peak Rainfall Intensity (1hrPRI)**
281 **increases. (a) April 2010-April 2012 (b) April 2010-April 2011 (c) April 2011-April 2012.**

282 **Figure 5: Seasonal and temporal effects on lahar probability. Contour graph of empirically-derived lahar probability**
283 **relative to the exceedance of One Hour Peak Rainfall Intensity (1hrPRI) thresholds in 6-month moving data windows**
284 **with 1-month staggered start dates. White numbers and dashed lines show temporal trends. Following the empirically-**
285 **derived 4 mm hr⁻¹ PRI contour, there is a 20% probability of a lahar if this threshold is exceeded at ① (6-month start**
286 **date of 13/10/2010). This probability increases to 38% at ② (13/04/2011); and declines to 18% at ③ (13/10/2011).**
287 **Alternatively, reading horizontally across the graph for a lahar probability of 38% the associated PRI threshold**
288 **increases from 4 mm hr⁻¹ at ② (13/04/2011) to approximately 15 mm hr⁻¹ at ④ (13/10/2011).**

289 **Figure 6: Assessment of binary logistic regression-based lahar probability estimation models in the Belham Valley,**
290 **Montserrat. (a) Illustration of four binary logistic regression-based lahar probability estimation models created from**
291 **Year 1, Year 2, Wet Season and Dry Season data. (b) ROC curves assessing the lahar forecasting performance of an**
292 **exclusively 1hrPRI-centric logistic regression-based lahar probability estimation model and a multi-variable (1hrPRI,**
293 **antecedent rainfall and long-term cumulative rainfall) model.**



294 **References**

295 Alexander, J., Barclay, J., Susnik, J., Loughlin, S. C., Herd, R. A., Darnell, A., and Crosweller, S.: Sediment-
296 charged flash floods on Montserrat: The influence of synchronous tephra fall and varying extent of vegetation
297 damage, *Journal of Volcanology and Geothermal Research*, 194, 127-138, 10.1016/j.jvolgeores.2010.05.002,
298 2010.

299 Auker, M. R., Sparks, R. S. J., Siebert, L., Crosweller, H. S., and Ewert, J.: A statistical analysis of the global
300 historical volcanic fatalities record, *Journal of Applied Volcanology*, 2, 10.1186/2191-5040-2-2, 2013.

301 Barclay, J., Johnstone, J. E., and Matthews, A. J.: Meteorological monitoring of an active volcano: Implications
302 for eruption prediction, *Journal of Volcanology and Geothermal Research*, 150, 339-358,
303 10.1016/j.jvolgeores.2005.07.020, 2006.

304 Barclay, J., Alexander, J., and Susnik, J.: Rainfall-induced lahars in the Belham Valley, Montserrat, West Indies,
305 *Journal of the Geological Society*, 164, 815-827, 10.1144/0016-76492006-078, 2007.

306 Bonadonna, C., Mayberry, G. C., Calder, E. S., Sparks, R. S. J., Choux, C., Jackson, P., Lejeune, A. M., Loughlin,
307 S. C., Norton, G. E., Rose, W. I., Ryan, G., and Young, S. R.: Tephra fallout in the eruption of Soufriere Hills
308 Volcano, Montserrat, *Geological Society, London, Memoirs*, 21, 483-516, 10.1144/gsl.mem.2002.021.01.22,
309 2002.

310 Capra, L., Borselli, L., Varley, N., Gavilanes-Ruiz, J. C., Norini, G., Sarocchi, D., Caballero, L., and Cortes, A.:
311 Rainfall-triggered lahars at Volcán de Colima, Mexico: Surface hydro-repellency as initiation process, *Journal of
312 Volcanology and Geothermal Research*, 189, 105-117, 10.1016/j.jvolgeores.2009.10.014, 2010.

313 Cole, P. D., Calder, E. S., Sparks, R. S. J., Clarke, A. B., Druitt, T. H., Young, S. R., Herd, R. A., Harford, C. L.,
314 and Norton, G. E.: Deposits from dome-collapse and fountain-collapse pyroclastic flows at Soufriere Hills
315 Volcano, Montserrat, *Geological Society, London, Memoirs*, 21, 231-262, 10.1144/gsl.mem.2002.021.01.11,
316 2002.

317 Collins, B. D., and Dunne, T.: Erosion of tephra from the 1980 eruption of Mount St Helens, *Geological Society
318 of America Bulletin*, 97, 896-905, 10.1130/0016-7606(1986)97<896:eotfte>2.0.co;2, 1986.

319 Fawcett, T.: An introduction to ROC analysis, *Pattern Recognition Letters*, 27, 861-874,
320 10.1016/j.patrec.2005.10.010, 2006.

321 Fohrer, N., Berkenhagen, J., Hecker, J. M., and Rudolph, A.: Changing soil and surface conditions during rainfall
322 - Single rainstorm/subsequent rainstorms, *CATENA*, 37, 355-375, Doi 10.1016/S0341-8162(99)00026-0, 1999.

323 Froude, M. J.: Lahar Dynamics in the Belham River Valley, Montserrat: Application of Remote Camera-Based
324 Monitoring for Improved Sedimentological Interpretation of Post-Event Deposits, *PhD Thesis, School of
325 Environmental Science, University of East Anglia*, 2015.

326 Graf, W. L.: The rate law in fluvial geomorphology, *American Journal of Science*, 277, 178-191, 1977.

327 Hosmer Jr, D. W., Lemeshow, S., and Sturdivant, R. X.: *Applied logistic regression*, John Wiley & Sons, 2013.

328 Iverson, R. M.: Landslide triggering by rain infiltration, *Water Resources Research*, 36, 1897-1910,
329 10.1029/2000wr900090, 2000.

330 Iverson, R. M., Reid, M. R., Logan, M., LaHusen, R. G., Godt, J. W., and Griswold, J. P.: Positive feedback and
331 momentum growth during debris-flow entrainment of wet bed sediment, *Nature Geoscience*, 4, 116-121,
332 10.1038/NGEO1040, 2011.



333 Jones, R., Manville, V., and Andrade, D.: Probabilistic analysis of rain-triggered lahar initiation at Tungurahua
334 volcano, *Bulletin of Volcanology*, 77, 10.1007/s00445-015-0946-7, 2015.

335 Komorowski, J. C., Legendre, Y., Christopher, T., Bernstein, M., Stewart, R., Joseph, E., Fournier, N., Chardot,
336 L., Finizola, A., Wadge, G., Syers, R., Williams, C., and Bass, V.: Insights into processes and deposits of
337 hazardous vulcanian explosions at Soufrière Hills Volcano during 2008 and 2009 (Montserrat, West Indies),
338 *Geophysical Research Letters*, 37, 10.1029/2010gl042558, 2010.

339 Lavigne, F., Thouret, J. C., Voight, B., Young, K., LaHusen, R., Marso, J., Suwa, H., Sumaryono, A., Sayudi, D.
340 S., and Dejean, M.: Instrumental lahar monitoring at Merapi Volcano, Central Java, Indonesia, *Journal of
341 Volcanology and Geothermal Research*, 100, 457-478, 10.1016/S0377-0273(00)00151-7, 2000.

342 Leavesley, G., Lusby, G., and Lichty, R.: Infiltration and erosion characteristics of selected tephra deposits from
343 the 1980 eruption of Mt St Helens, Washington, USA, *Hydrological Sciences*, 34, 339-353, 1989.

344 Major, J. J., and Yamakoshi, T.: Decadal-scale change of infiltration characteristics of a tephra-mantled hillslope
345 at Mount St Helens, Washington, *Hydrological Processes*, 19, 3621-3630, 10.1002/Hyp.5863, 2005.

346 Major, J. J., Pierson, T. C., Dinehart, R. L., and Costa, J. E.: Sediment yield following severe volcanic disturbance
347 - A two-decade perspective from Mount St. Helens, *Geology*, 28, 819-822, 10.1130/0091-
348 7613(2000)28<819:Syfsvd>2.0.Co;2, 2000.

349 Manville, V., Hodgson, K. A., Houghton, B. F., Keys, J. R. H., and White, J. D. L.: Tephra, snow and water:
350 complex sedimentary responses at an active, snow-capped stratovolcano, Ruapehu, New Zealand, *Bulletin of
351 Volcanology*, 62, 278-293, 2000.

352 Marcial, S., Melosantos, A., Hadley, K., LaHusen, R., and Marso, J.: Instrumental Lahar Monitoring at Mount
353 Pinatubo, in: *Fire and Mud, Eruptions and Lahars of Mt Pinatubo, Philippines*, edited by: Newhall, C., and
354 Punongbayan, R., PHIVOLCS/University of Washington Press, Quezon City/Seattle, 1015-1023, 1996.

355 Mead, S., Magill, C., and Hilton, J.: Rain-triggered lahar susceptibility using a shallow landslide and surface
356 erosion model, *Geomorphology*, 273, 168-177, 10.1016/j.geomorph.2016.08.022, 2016.

357 Ogawa, Y., Daimaru, H., and Shimizu, A.: Experimental study of post-eruption overland flow and sediment load
358 from slopes overlain by pyroclastic-flow deposits, Unzen volcano, Japan, *Géomorphologie : relief, processus,
359 environnement*, 13, 237-246, 10.4000/geomorphologie.3962, 2007.

360 Pierson, T. C., and Major, J. J.: Hydrogeomorphic effects of explosive volcanic eruptions on drainage basins,
361 *Annual Review of Earth and Planetary Sciences*, 42, 469-507, 10.1146/annurev-earth-060313-054913, 2014.

362 Rodolfo, K., and Arguden, A.: Rain-lahar generation and sediment-delivery systems at Mayon Volcano,
363 Philippines, in: *Sedimentation in Volcanic Settings*, edited by: Fisher, R., and Smith, G., SEPM, Special
364 Publication 45, 71-87, 1991.

365 Schumm, S. A., and Rea, D. K.: Sediment Yield from Disturbed Earth Systems, *Geology*, 23, 391-394,
366 10.1130/0091-7613(1995)023<0391:Syfdes>2.3.Co;2, 1995.

367 Segerstrom, K.: Erosion studies at Paricutin, State of Michoacan, Mexico, *USGS Bulletin*, 965-A, 164 pp, 1950.

368 Smith, G. A., and Fritz, W. J.: Volcanic influences on terrestrial sedimentation, *Geology*, 17, 375-376, 1989.

369 Stinton, A. J., Cole, P. D., Stewart, R. C., Odbert, H. M., and Smith, P.: The 11 February 2010 partial dome
370 collapse at Soufrière Hills Volcano, Montserrat, *Geological Society, London, Memoirs*, 39, 133-152,
371 10.1144/m39.7, 2014.

372 Thouret, J. C., Oehler, J. F., Gupta, A., Solikhin, A., and Procter, J. N.: Erosion and aggradation on persistently
373 active volcanoes-a case study from Semeru Volcano, Indonesia, *Bulletin of Volcanology*, 76, 10.1007/S00445-
374 014-0857-Z, 2014.



375 Todisco, F.: The internal structure of erosive and non-erosive storm events for interpretation of erosive processes
376 and rainfall simulation, *Journal of Hydrology*, 519, 3651-3663, 10.1016/j.jhydrol.2014.11.002, 2014.

377 Waldron, H. H.: Debris flow and erosion control problems caused by the ash eruptions of Irazu Volcano, Costa
378 Rica, United States Geological Survey, *Bulletin* 1241-I, 37 p., 1967.

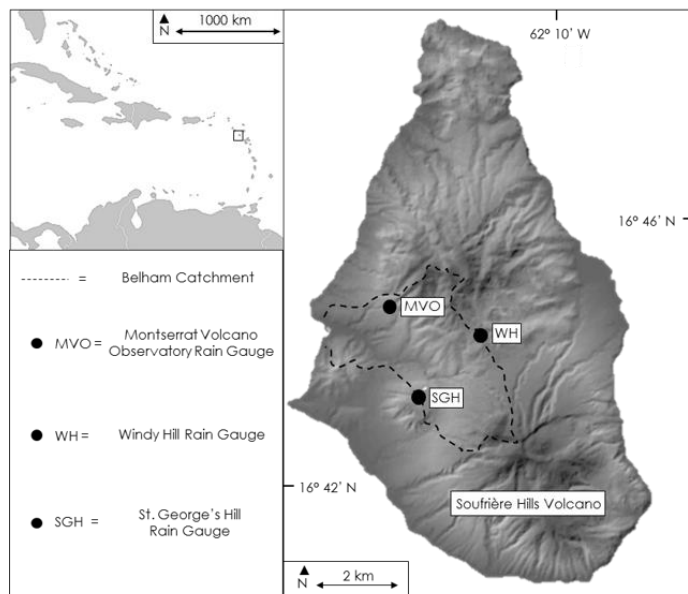
379 Wang, B., Kim, H.-J., Kikuchi, K., and Kitoh, A.: Diagnostic metrics for evaluation of annual and diurnal cycles,
380 *Climate Dynamics*, 37, 941-955, 10.1007/s00382-010-0877-0, 2010.

381 Wischmeier, W., and Smith, D.: Predicting rainfall erosion losses - A guide to conservation planning, *Agricultural
382 Handbooks (USA)* No. 537, US Department of Agriculture, Washington DC, 1978.

383 Yamakoshi, T., and Suwa, H.: Post-eruption characteristics of surface runoff and sediment discharge on the slopes
384 of pyroclastic-flow deposits, Mt Unzen, Japan, *Transactions, Japanese Geomorphological Union*, 21, 469-497,
385 2000.



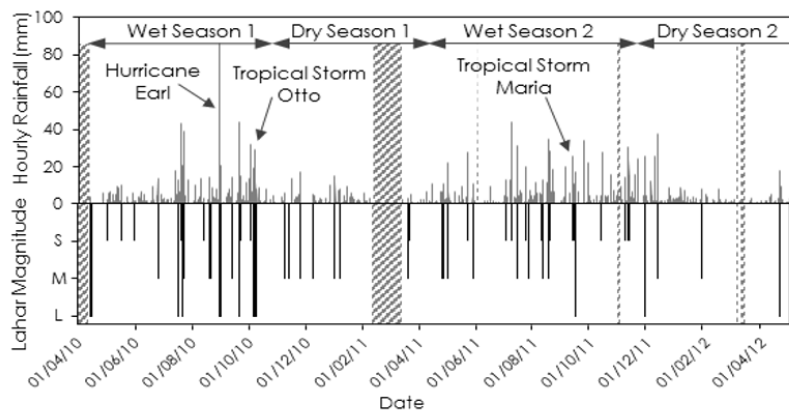
386 Fig.1



387



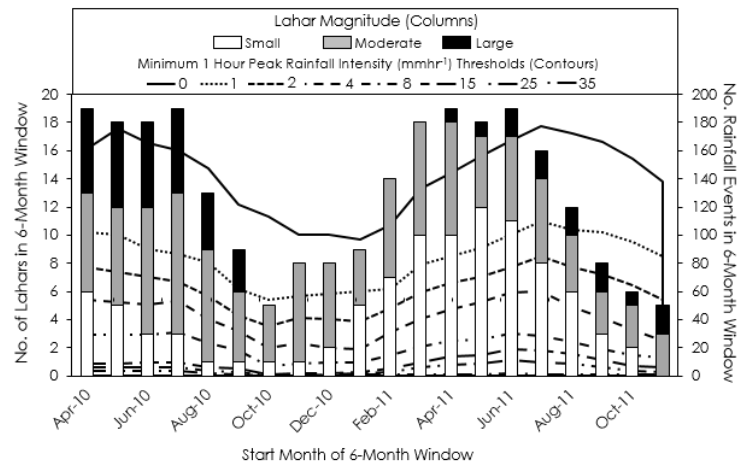
388 Fig.2



389



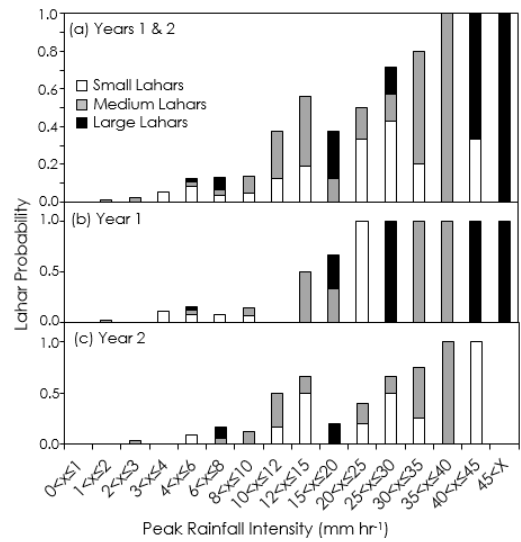
390 Fig. 3



391



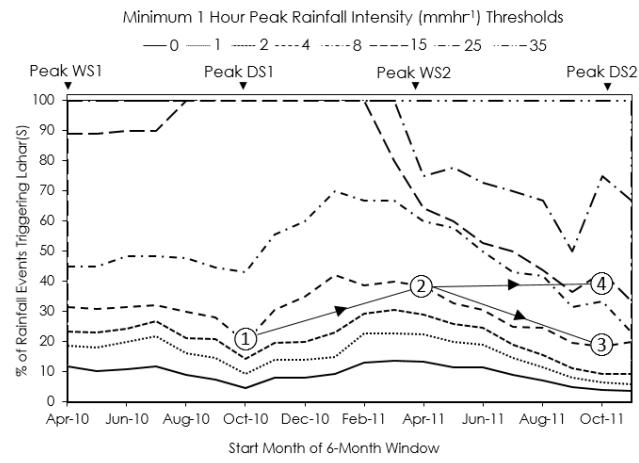
392 Fig. 4



393



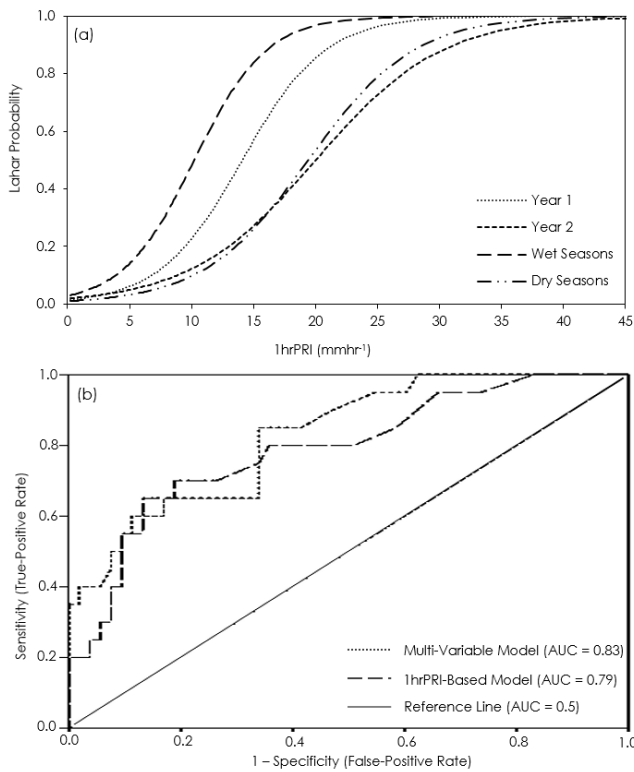
394 Fig. 5



395



396 Fig. 6



397